Emergent dimensional reduction of the spin sector in a model for narrow-band manganites

Shuhua Liang,[1,2] Maria Daghofer,[3,*] Shuai Dong,[4] Cengiz Şen,[1,2] and Elbio Dagotto[1,2]
[1]*Department of Physics and Astronomy, The University of Tennessee, Knoxville, TN 37996, USA*
[2]*Materials Science and Technology Division, Oak Ridge National Laboratory, Oak Ridge, TN 32831, USA*
[3]*IFW Dresden, P.O. Box 27 01 16, D-01171 Dresden, Germany*
[4]*Department of Physics, Southeast University, Nanjing 211189, China*
(Received 11 May 2011; published 6 July 2011)

The widely used double-exchange model for manganites is shown to support various "striped" phases at filling fractions $1/n$ ($n = 3, 4, 5, \ldots$), in the previously unexplored regime of narrow bandwidth and small Jahn-Teller coupling. Working in two dimensions, our main result is that these stripes can be individually spin flipped without a physically relevant change in the energy, i.e., we find a large ground-state manifold with nearly degenerate energies. The two-dimensional spin system thus displays an unexpected dynamically generated dimensional reduction into decoupled one-dimensional stripes, even though the electronic states remain two dimensional. Relations of our results with recent literature addressing compass models in quantum computing are discussed.

DOI: 10.1103/PhysRevB.84.024408 PACS number(s): 75.25.Dk, 71.10.Hf, 75.47.Lx

I. INTRODUCTION

The manganite family of Mn-oxide materials has attracted considerable attention mainly due to the colossal magnetoresistance effect, where a magnetic field hugely enhances the electrical conductivity.[1] More recently, multiferroicity has been found in some members of this family, particularly, when chemical substitution reduces the bandwidth of the mobile electrons. Magnetic multiferroicity, where a ferroelectric (FE) polarization is induced by the magnetic order, has lately been intensively investigated.[2–4] Furthermore, manganites provide a fertile ground to study various ordered phases where magnetic, orbital, and charge degrees of freedom interact and compete. As a result of the large number of tendencies simultaneously active on comparable energy scales, phases with very different physical properties can nevertheless be very close in energy.[5,6]

The competition of all these active degrees of freedom often leads to "striped" phases where electron motion is confined to one-dimensional (1D) subspaces. In manganites at large hole doping, for example, electrons mainly occupy orbitals that point along either the x or the y direction. Spins then order ferromagnetically along this direction, because this favors the electronic kinetic energy via the double-exchange (DE) mechanism. In the other direction, where the electronic motion is suppressed, then DE is not active, and antiferromagnetic (AF) superexchange dominates. This establishes AF spin correlations, leading to the "spin striped" C-type AF phase.[1,7–10] Other examples involve the ferromagnetic (FM) zigzag chains, which are antiferromagnetically coupled among themselves, that form the well-known CE-AF phase at half filling or the E-AF phase in the undoped limit.[1] The ground state of these phases usually have collinear magnetic order, i.e., alignment between any two spins is either perfectly FM or AF. Another aspect to note is that while the electronic kinetic energy is 1D, the magnetic order is fully two dimensional (2D), with AF order between the chains mediated by superexchange (SE). In the absence of AF SE, a completely FM state with 2D electron motion is energetically favorable.

Recently, some of us predicted the existence of a new multiferroic phase, dubbed *spin-orthogonal stripe* (SOS) phase, located in the previously unexplored region of quarter-hole doping, small Jahn-Teller electron-lattice coupling, and narrow e_g-electron bandwidth.[11] In contrast to the "striped" phases mentioned above, the competition between FM DE and AF SE stabilizes *noncollinear* magnetic order on some bonds, where the nearest-neighbor (NN) t_{2g} spins are orthogonal to one another. As in an analogous half-doped noncollinear phase,[12] this competition is expected to lead to a relatively high multiferroic critical temperature ($\sim$100 K). These phases can be visualized as composed of "thick" stripes, where all magnetic correlations within a stripe are collinear, i.e., AF or FM, while adjacent stripes display noncollinear spins.

In the present publication, we report that the SOS phase described above, as well as similar phases at dopings $x = 1/n$ with integer $n > 2$, have another unexpected property, namely, a very highly degenerate ground-state manifold. We find that the spins of any collinear stripe can be rotated without a significant change in energy, as long as the spins in adjacent stripes remain orthogonal. Spins in next-nearest-neighbor stripes can thus be at arbitrary angles relative to each other, implying that there is no magnetic order in the direction perpendicular to the stripes. Analogous *dimensional reduction* effects on the magnetic order, where a higher dimensional (2D in our case) spin system decouples into lower dimensional (1D) subsystems, have been experimentally observed in other contexts such as near a quantum-critical point.[13] Three-dimensional spin-ice systems[14] also show macroscopic degeneracy, and they can decouple into 2D planes when a magnetic field "switches off" some spins connecting the planes.[15,16]

In contrast to spin ice, where a local symmetry allows two states for each tetrahedron, leading to a macroscopic ground-state degeneracy and an extensive entropy proportional to the system size N, the near degeneracy reported here is not quite macroscopic. The degeneracy involves flipping or rotating whole stripes, and the number of stripes in the 2D plane grows with the square root of the system size. This indicates that the emergent degeneracy of the ground state is intermediate between local and global. Similar intermediate symmetry effects connected to dimensional reduction have been extensively discussed in orbital-only models, as well as in the context of quantum computation. An example is

the so-called "compass-model" where the $x(y)$ components of the orbital pseudospins are coupled Ising-like in the $x(y)$ direction. This model was originally introduced to capture the frustrated hoppings of the e_g orbitals of manganites.[17] Its low-energy states are ordered along only one dimension,[18,19] implying a symmetry that, again, is intermediate between local and global.[19,20]

Even though the compass model was originally suggested to model the frustration inherent in degenerate e_g orbitals in 2D, the actual (partially frustrated) Hamiltonian describing these orbitals does not exhibit such a high degeneracy. In fact, it has been shown that the peculiar properties of the compass model are sensitive to even rather slight modifications of the Hamiltonian and that a unique ground state with alternating orbital order sets easily when the model is modified toward a more realistic description of 2D e_g systems.[21] In three dimensions, on the other hand, the model with a realistic e_g-orbital structure does decouple into *planes*,[22–24] as long as the magnetic order is fully FM. Once the magnetic degree of freedom is included, however, the ground state turns out to show AF order along the z direction. This changes the relevant orbital Hamiltonian and as a consequence three-dimensional spin-orbital order with a nondegenerate ground state is stabilized. In addition to the e_g orbital degrees of freedom in manganites, heavier elements with a strong relativistic spin-orbit interaction were discussed as a possible realization of compass models.[25] However, here an isotropic Heisenberg term due to Hund's coupling would likely be present as well,[26] again inducing 2D order without $2^{\sqrt{N}}$ degeneracy.[27] Finally, it was pointed out that the compass model describes properties desired for fault-tolerant qbits,[19,28] and coupled Josephson-junction arrays have been implemented for this purpose.[29]

The directional ordering described by the compass model is thus potentially very interesting, but dedicated Josephson-junction arrays appear so far the only systems showing such an effect. In the condensed-matter systems conjectured to display this physics based on particular features of their low-energy Hamiltonians, additional—even rather small[27]—perturbations, as often present in realistic descriptions of materials, have thus far been found to lift the high degeneracy. It has been suggested that the *opposite* route might work, i.e., a more complex Hamiltonian, which does not itself have the appropriate symmetry intermediate between local and global, might still support a ground-state manifold that *has* such symmetries.[20,30,31] As mentioned above, some experimental evidence of such behavior exists,[13] and a similar effect is known in the case of spin ice.[15,16] However, we are not aware of any model where "compass-like" behavior has been shown to emerge effectively for the ground-state manifold. We present here an unbiased numerical study showing this to happen in a Hamiltonian realistic for manganites, in a particular region of parameter space.

Section II contains the Model, which describes not only the e_g orbital system at the origin of the compass model, but also includes the spin and even the coupling to lattice distortions. In Sec. III, the numerical techniques are presented. In Sec. IV, we show that the 2D spin system effectively decomposes into uncoupled 1D stripes, while the electronic kinetic energy remains fully 2D. We also discuss orbital occupation and the relation between the magnetic degeneracy and dispersionless electronic states.

II. MODEL

The Hamiltonian considered here has been extensively studied in the past decade, and it has been shown to be very helpful to understand the complex behavior of manganites. In particular, the model reproduces the large variety of phases observed in manganites, e.g., A-type AF, C-type AF, FM, CE-AF, or E-AF, and also the colossal-magnetoresistance regime.[1] The Hamiltonian is given by

$$H = -\sum_{\langle ij\rangle \| x/y}^{\alpha,\beta} t_{x/y}^{\alpha\beta}(\Omega_{ij} c_{i\alpha}^{\dagger} c_{j\beta} + H.c.) + J_{\rm AF}\sum_{\langle ij\rangle} \vec{S}_i \cdot \vec{S}_j + \lambda \sum_i \left(- Q_{1i} n_i + Q_{2i}\tau_i^x + Q_{3i}\tau_i^z \right) + \frac{1}{2}\sum_i \left(2Q_{1i}^2 + Q_{2i}^2 + Q_{3i}^2\right). \quad (1)$$

The first term gives the kinetic energy of electrons in the two e_g orbitals, containing the electronic hopping on NN bonds $\langle ij\rangle$ along the x and y directions (we study a 2D lattice for simplicity). The operator $c_{i\alpha}^{\dagger}$ ($c_{i\alpha}$) creates (annihilates) an electron at site i and at orbital α, where the orbital indices α and β run over the $d_{x^2-y^2}$ and $d_{3r^2-z^2}$ orbitals of the Mn ions. The orbital- and direction-dependent hopping parameters are given by

$$t_x^{\alpha\beta} = \begin{pmatrix} \frac{3}{4} & -\frac{\sqrt{3}}{4} \\ -\frac{\sqrt{3}}{4} & \frac{1}{4} \end{pmatrix} t_0, \quad t_y^{\alpha\beta} = \begin{pmatrix} \frac{3}{4} & +\frac{\sqrt{3}}{4} \\ +\frac{\sqrt{3}}{4} & \frac{1}{4} \end{pmatrix} t_0, \quad (2)$$

where the interorbital hoppings are negative (positive) on bonds along the $x(y)$ direction, and $t_0 = 0.2$–0.5 eV defines the energy unit.[1] The Hund's coupling, which links the itinerant electrons to localized t_{2g} spins, is here taken to be infinite for simplicity, which implies that the e_g electrons' spin is always parallel to the local t_{2g} spin. Neither Hund's rule coupling nor the electron spin thus appear explicitly in the Hamiltonian. This approach leads to a modification of the bare hopping that is captured by a (complex) Berry phase factor

$$\Omega_{ij} = \cos\frac{\theta_i}{2}\cos\frac{\theta_j}{2} + \sin\frac{\theta_i}{2}\sin\frac{\theta_j}{2} e^{-i(\phi_i-\phi_j)}, \quad (3)$$

which depends on the angles θ_i, ϕ_i and θ_j, ϕ_j that define the classical localized spins at sites i and j.[32] Between sites with parallel (antiparallel) t_{2g} spins, the Berry phase factor becomes one (zero), implying that the kinetic energy favors parallel spins due to the DE mechanism. Between noncollinear spins, i.e., spins with a relative angle between 0° and 180°, its absolute value is between 0 and 1, and it can be negative or even complex.

The second term of Eq. (1) describes the direct AF SE coupling between NN t_{2g} spins. The third term represents the coupling of e_g electrons with the lattice, via the Jahn-Teller (JT) (Q_2 and Q_3) and breathing (Q_1) modes. λ is a dimensionless lattice-electron coupling coefficient. Only the x–y plane distortions are considered here, and if the overall

lattice shape (square) can be assumed not to change, Q_1 can be set to $-\sqrt{2}Q_3$. The lattice normal modes Q_2 and Q_3 are related to shifts δ^x, δ^y ($\delta^z = 0$) of the coordinates of the six oxygens surrounding each manganese via $Q_2 = (\delta^x - \delta^y)/\sqrt{2}$ and $Q_3 = -(\delta^x + \delta^y)/\sqrt{6}$. $n_{i\alpha} = c^\dagger_{i\alpha} c_{i\alpha}$ and $n_i = n_{i,x^2-y^2} + n_{i,3z^2-r^2}$ are density operators; while

$$\tau_i^z = \frac{(n_{i,x^2-y^2} - n_{i,3z^2-r^2})}{2}, \tag{4}$$

$$\tau_i^x = \frac{(c^\dagger_{i,x^2-y^2} c_{i,3z^2-r^2} + c^\dagger_{i,3z^2-r^2} c_{i,x^2-y^2})}{2}, \tag{5}$$

denote the orbital pseudospin operators, similar to the Pauli matrices for spins.[1] The lattice distortions are thus coupled to the orbital degree of freedom. Undoped manganites correspond to a filling of one electron per Mn, while doping x and filling n are related via $n = 1 - x$.

III. METHODS

Markov-chain Monte Carlo (MCMC), zero-T optimization, and variational methods were used to study the ground-state and low-temperature properties of the Hamiltonian Eq. (1). This Hamiltonian couples noninteracting electrons to the classical variables $\vec{q}_i = \{\theta_i, \phi_i, \delta_i^x, \delta_i^y\}$ describing the localized spins and lattice distortions. For any set of $\vec{q}$'s, Eq. (1) is diagonalized using standard library routines, and the free energy of the electronic system can be easily evaluated via the usual equations from statistical physics. The energy is then used in a conventional MCMC procedure to determine whether a new set of $\vec{q}_i$ should be accepted, as detailed in various publications.[1] Since care must be taken that the results are independent from the initial configuration and that thermal equilibrium has been reached, such MCMC simulations are quite CPU-time consuming. Their huge advantage is that they are *unbiased*, meaning that, for long enough run time, they will converge to the true relevant state of the cluster under study, regardless of the initial state used. We employed this method on 6×6 lattices to obtain the phase diagram in the λ–$J_{\rm AF}$ plane, and on 12×12 lattices for a selected number of points.

The MCMC is complemented by the zero-T optimization method where the $\vec{q}$'s are optimized to reach the lowest possible energy by employing the derivatives $\frac{\partial H(q)}{\partial q}$, as detailed in Ref. 33. This optimization method is particularly useful around a local energy minimum, where it reaches higher precision than the MCMC and is, thus, efficiently combined with MCMC, which is better at finding the *global* minimum. Finally, we also complement these studies by a variational comparison of the energies of fixed configurations of classical spins and lattice distortions. While the variational approach is not unbiased, because only chosen configurations were combined, it is valuable, because far larger lattices can be reached; it was employed, e.g., to verify that various $\rm SOS_{1/3}$ configurations indeed are practically degenerate. In addition to $L \times L$ squares, this approach was also employed on $\sqrt{2}L_1 \times \sqrt{2}L_2$ rectangles. Periodic boundary conditions were used in MCMC and optimization, and for variational energy comparison. To calculate selected observables, such as the spin-structure factor and the density of states, we additionally used twisted boundary conditions leading to a denser k mesh, as described in, e.g., Ref. 34.

IV. RESULTS

Motivated by the recent prediction of the $x = 1/4$ SOS phase,[11] and of a similar phase at half doping,[12] we have investigated other fillings $x = 1/3, 1/5, \ldots$, focusing here on parameters relevant to narrow-band manganites. The discussion below mainly focuses on results for $x = 1/3$, where the SOS phase has narrower stripes than for smaller x and can thus be investigated on smaller clusters. A variational energy comparison and some MCMC studies were also performed for $n \geqslant 5$, leading to analogous results.

A. Phase diagram and highly degenerate ground state manifold

Figure 1(a) shows a snapshot obtained in a MCMC run for $J_{\rm AF} = 0.19t_0$ and $\lambda = 0$, where the spins happened to lie almost within the x–y plane. It illustrates the SOS phase expected for a filling of $1/3$, actually just one of its realizations, see the discussion below. As discussed for $x = 1/4$,[11] the SOS phase consists of domains of the E-AF phase of undoped manganites [illustrated in Fig. 1(b)], with spins rotated by 90° between neighboring domains. Each domain can be visualized as one "stripe," see Fig. 1(a), and the spins are then collinear within each of the stripes (regions between a pair of dashed lines), but between stripes they are orthogonal to each other. In Fig. 2, the ground-state energy of the $\rm SOS_{1/3}$ phase is compared to that of various other phases in the absence of electron-phonon coupling ($\lambda = 0$), and it is clear that the $\rm SOS_{1/3}$ phase has the lowest energy for a range of $J_{\rm AF}$. This is corroborated by data points obtained with unbiased MCMC, which closely follow the variational energies, indicating that the true ground state has been found.

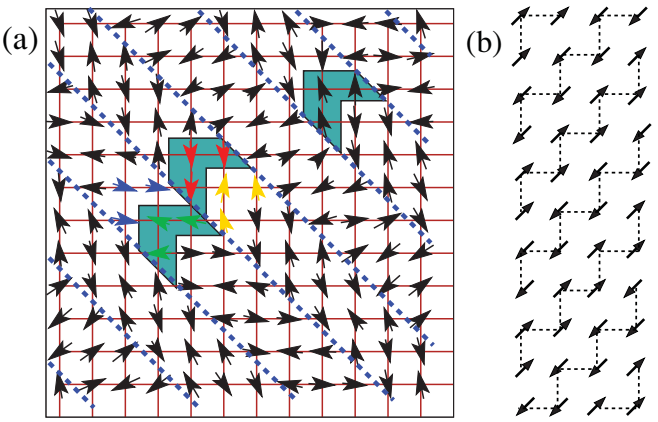

FIG. 1. (Color online) (a) Monte-Carlo snapshot for $J_{\rm AF} = 0.19t_0$, $\lambda = 0$, and $\beta t_0 = 1200$, in the regime of the $\rm SOS_{1/3}$ phase. It can be visualized as composed of domains of the E-AF phase illustrated in the cartoon (b). (a) NN domains ("stripes") are separated by dashed lines, they have spins at right angles. (b) Dashed lines indicate the zigzag FM chains of the E-AF phase; in (a) shading (color) indicates a few of the short segments of the E-phase zigzag chains that survive in the $\rm SOS_{1/3}$ phase, later called "arrows."

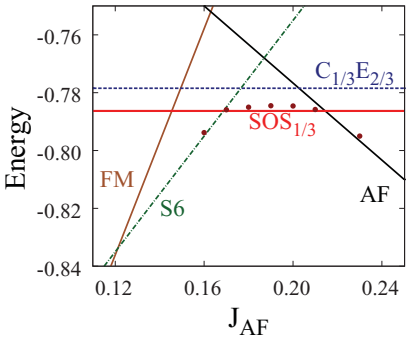

FIG. 2. (Color online) Zero temperature ($T = 0$) energies (per site) of several magnetic phases, at doping $x = 1/3$ and $\lambda = 0$, vs J_{AF}. Dots represent MCMC results at $T = 0.002$ on a 6×6 lattice that closely follows the variational results. S6 denotes a spiral phase with a period of 6 lattice spacings (Ref. 35), while a 12×12 lattices shows one with period 12; this phase thus converges to FM order with increasing lattice sizes (Ref. 36).

The phase diagram including electron-phonon coupling λ in addition to J_{AF} is given in Fig. 3, and it shows that the $SOS_{1/3}$ phase remains a stable ground state for $\lambda \lesssim 0.7$. As it may be expected, DE drives a FM metallic state at smaller J_{AF}, while large J_{AF} stabilizes a fully G-type AF phase. At large λ and intermediate J_{AF}, the $SOS_{1/3}$ phase is replaced by a variant of the exotic but well studied[1,6] CE phase.

However, our main result is that our calculations have revealed that this ground state is *not unique*: if all spins within one stripe are flipped by 180° (i.e., inverted), the total energy remains nearly unchanged. This is illustrated in Figs. 4(a) and 4(b), where two almost degenerate variants of the $SOS_{1/3}$ phase are illustrated. Taking into account noncoplanar spin configurations as well, the spins in each stripe can in fact be

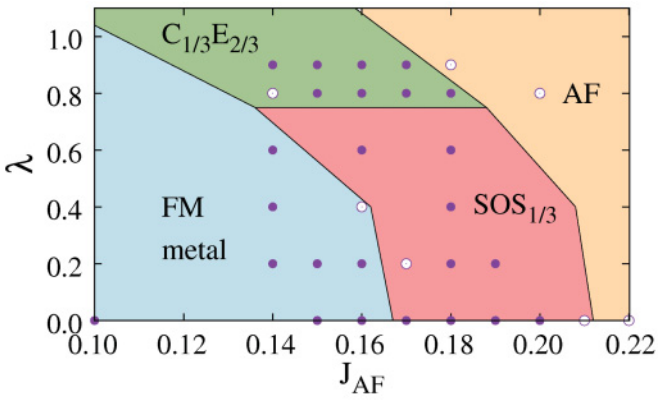

FIG. 3. (Color online) Zero-T phase diagram of model Eq. (1) at $x = 1/3$, varying λ and J_{AF}. Variational technique results are shown with shading (colors). The FM DE metallic phase dominates; large J_{AF} stabilizes AF phases. The "$C_{1/3}E_{2/3}$" phase is a variant (Refs. 6 and 11) of the CE phase at half filling (Ref. 1). The $SOS_{1/3}$ phase at intermediate J_{AF} and small λ is analogous to the $x = 1/4$ $SOS_{1/4}$ phase (Ref. 11), and is *highly degenerate*. Full dots show where MCMC (for 6×6 sites) confirmed the results; open dots are MCMC results that remained inconclusive due to metastabilities caused by phase competition. For details see Ref. 11.

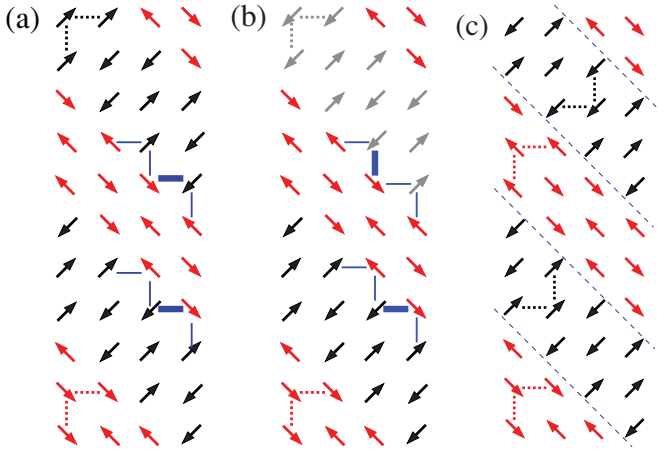

FIG. 4. (Color online) Cartoon for the spin patterns for two quasidegenerate states of the $SOS_{1/3}$ phase (a) and (b). Lines between domains with orthogonal spins illustrate the periodic pattern of Berry phases: thin lines denote positive sign and thick lines denote negative sign. The pattern in (b) is reached by flipping all spins in the top black stripe of (a), which entails changes in the signs of the Berry phases, but induces an energy difference of only $10^{-5}t_0$. The dotted lines connecting three ferromagnetically aligned spins indicate "arrows" of the E phase, see Fig. 1. In the pattern in (c), "arrows" in adjacent domains point in opposite directions. The energy per site in this phase is $10^{-2}t_0$ higher than that of the $SOS_{1/3}$ phase; flipping spins of one stripe induces energy differences of $\approx 5 \times 10^{-4}t_0$, i.e., at least 50 times larger than between (a) and (b).

rotated by any angle, as long as the spins in adjacent stripes remain orthogonal.

On square clusters, the difference in energy per site before and after a stripe spin flip is merely $\sim 10^{-5}t_0$ for flipping one stripe of a 12×12 lattice. This is 3 orders of magnitude smaller than the energy differences with other states shown in Fig. 2; similar conclusions were reached using tilted rectangles. Finite electron-phonon coupling $\lambda > 0$ as well as finite Hund's rule coupling $J_{\text{Hund}} < \infty$ leave the near degeneracy intact. Even rather small Hund's coupling $6t_0 \approx 1.2$ eV increases the energy split only to $\approx 5 \times 10^{-5}t_0$, still more than 2 orders of magnitude smaller than the energy differences to other phases ($\lambda \gtrsim 0.7t_0$ eventually drives a transition to the $C_{1/3}E_{2/3}$ state, see Fig. 3).

B. Magnetic, orbital, and charge patterns

Effectively, the 2D system decouples into 1D stripes, whose direction can be rotated independently from the other stripes as long as spins in NN stripes are at right angles. The relative orientation of stripes at larger distance is thus arbitrary and the spin structure factor $S(\mathbf{k})$ is finite along a whole *line* in momentum space, see Fig. 5(b), similar to results for the compass model.[27] The $S(\mathbf{k})$ modulation is due to the width of a double stripe.

Since spins on all bonds between stripes are orthogonal, the absolute value of the hopping connecting the stripes is the same in all realizations of the $SOS_{1/3}$ phase, with $|\Omega_{ij}| = 1/\sqrt{2}$ obtained from Eq. (3). However, having the same $|\Omega_{ij}|$ is not enough to establish such a degeneracy, as the complex phase of the Berry phase, in general, cannot be neglected. In the

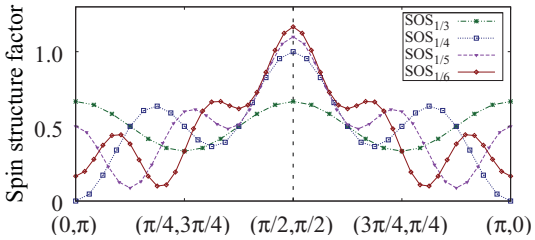

FIG. 5. (Color online) Spin-structure factor $S(\mathbf{k})$ along the line $(\pi,0)$ to $(0,\pi)$, calculated for the $SOS_{1/3}$ phase by averaging over all 2^{16} degenerate realizations with stripes along one direction of a $24\sqrt{2}\times\sqrt{2}$ cluster ($\lambda = 0$). $S(\mathbf{k}) \approx 0$ for all $\mathbf{k}$ except the line running from $(\pi,0)$ to $(0,\pi)$. Results at $x = 1/4$, $1/5$, and $1/6$ are also shown.

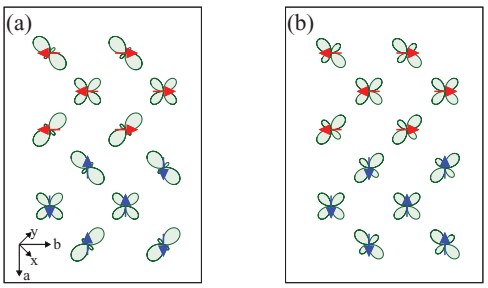

FIG. 6. (Color online) (a) Zero-T spin and orbital ordering of the $SOS_{1/3}$ phase, the ground state for $0.17 \lesssim J_{AF} \lesssim 0.21$ ($\lambda = 0$), see Fig. 3. For each site, the linear combination $|\alpha\rangle = \cos\alpha|3z^2 - r^2\rangle + \sin\alpha|x^2 - y^2\rangle$ is depicted that has the highest density, i.e., for the value of α maximizing $n_{i,\alpha}$. (b) The orbital with maximal density is shown for the modified $SOS_{1/3}$ phase with the spin pattern given in Fig. 4(c). While the depicted orbital is the one with the highest density, these cartoons do not fully describe the orbital states, as some density is also found in the orthogonal orbitals, see text.

"flux" phase,[37] NN spins are always orthogonal and flipping a spin would not change this; but there is nevertheless a unique ground state stabilized by the Berry phase. Similarly, flipping a stripe of the "$SOS_{1/2}$" phase at half doping[12] preserves the absolute value of all hoppings, yet costs far more energy than flipping a stripe of the $SOS_{1/3}$ phase. In order to show that the ground-state degeneracy is not due solely to having orthogonal spins, it is illustrative to analyze the "modified" $SOS_{1/3}$ phase depicted in Fig. 4(c). Similar to the actual $SOS_{1/3}$ phase, this phase is made up of domains of the E-AF phase that are orthogonal to each other. The only difference is that the "arrows" formed by the FM spins point in opposite directions in adjacent stripes in this modified phase. Even though the spins along the boundaries between stripes are the same in both phases, the modified phase has a higher energy per site by $10^{-2}t_0$, which is larger than that of the energy difference to the $C_{1/3}E_{2/3}$ phase, see Fig. 2, indicating that the internal composition of the stripes matters as much as their boundaries. Moreover, the modified phase does not show such a near perfect degeneracy, as flipping a stripe on a 12×12 lattice costs $\approx 5\times 10^{-4}t_0$, and while this is not a large energy difference, it is at least 50 times as much as for the $SOS_{1/3}$ phase.

The dominant orbital occupancy and its relation to the spin pattern is shown in Fig. 6. The building block of the $SOS_{1/3}$ phase is an arrow made of three FM spins, with a "center" and two "wings" that point in the x and y directions. For each site, one can calculate the dominant linear combination of the two e_g orbitals, i.e., the orbital with the highest density. At the wings of the arrows, these are the directional orbitals pointing to the center, because they can maximize the kinetic energy along the FM bond,[1] see Fig. 6; they are half filled. On the central site, the $x^2 - y^2$ orbital dominates due to its large overlap with adjacent sites. However, it turns out that the electronic configuration of the $SOS_{1/3}$ phase cannot be fully characterized in terms of singly occupied orbitals, which is reminiscent of the edge sites in the CE phase.[38] Even though the depicted orbitals have the highest density, some electronic weight is also found in the orthogonal states and Fig. 6(a) only partially describes the orbital state. In the center, the explicit occupancies are thus $n_{x^2-y^2} = 0.4$ and $n_{3z^2-r^2} = 0.28$, and in the "wings" along x/y, we find $n_{y^2-z^2/z^2-x^2} = 0.24$ in addition to $n_{3x^2-r^2/3y^2-r^2} = 0.5$. The total density is the sum of the two orbital densities on each site, and shows only weak stripe modulation, with $n = 0.68$ in the center and $n = 0.66$ in the wings.

The relatively large density $n_{y^2-z^2} = 0.24$ in a "wing" pointing along x may seem surprising, as the $y^2 - z^2$ orbital cannot hop along the FM bond directed along x to the center.[1] However, it can hop with an only slightly reduced amplitude $|\Omega_{ij}| = 1/\sqrt{2}$ to an adjacent stripe. This process becomes even more important in the modified $SOS_{1/3}$ phase of Fig. 4(c), whose dominant orbitals are shown in Fig. 6(b). In this case, the $1/\sqrt{2}$ interstripe hopping connects two directional $3x^2 - r^2$ (or $3y^2 - r^2$) orbitals with a large overlap. We will discuss in the next section (Sec. IV C) why the hoppings between stripes cannot be neglected in either phase.

C. Two-dimensional kinetic energy and dispersionless states

As discussed above, the effective hoppings with their Berry phases are not the same in the various (almost) degenerate states of the $SOS_{1/3}$ phase. It may be tempting to believe that one can find a local gauge transformation that transforms the sign patters of one realization into that of another, with a flipped stripe. In this case, the electronic Hamiltonians would be equivalent and thus have the same eigenenergies, explaining the degeneracy. However, the density of states shown in Fig. 7 is very different for different $SOS_{1/3}$ patterns, indicating that the eigenenergies of their electronic Hamiltonians are in fact quite different.

That the different $SOS_{1/3}$ configurations have different electronic Hamiltonians can also be inferred from the one-particle spectral density $A(\mathbf{k},\omega)$ shown in Fig. 8. One aspect to note is that the occupied states do not show any (quasi-) 1D character, and the states are dispersive both along the stripes $[(0,0)$–$(\pi,\pi)]$ and perpendicular to them $[(0,0)$–$(\pi,-\pi)]$. In fact, the kinetic energy between the stripes is necessary for the $SOS_{1/3}$ phase, as the orthogonal spin arrangements are stabilized by the competition between the FM DE and AF SE processes. Electrons cannot hop directly along the stripes, as NN spins are AF ordered, but they move along this direction via

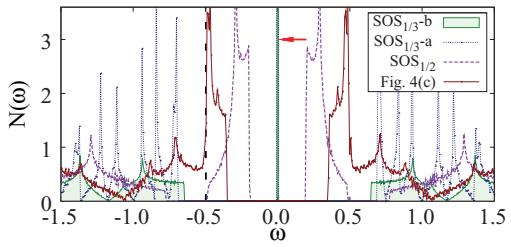

FIG. 7. (Color online) (a) Density of states $N(\omega)$ ($\lambda = 0$) for two patterns of the $SOS_{1/3}$ phase, the phase shown in Fig. 4(c), and the $SOS_{1/2}$ phase (Ref. 12). The arrow indicates the dispersionless states of the $SOS_{1/3}$ phases.

neighboring stripes, leading to a somewhat weaker dispersion than perpendicular to the stripes.

The spectral density of the $SOS_{1/3}$ phase in Fig. 8 can be compared to that of a toy model where all hoppings are replaced by their absolute values. As can be seen in Fig. 9, the spectral density then consists of six coherent bands (the dispersionless band at $\omega = 0$ is doubly degenerate) corresponding to six states formed by the two orbitals of three sites within each arrow. The results for the full model in Fig. 8 shows some remnants of these bands, especially around (0,0) and (π,π). At other momenta, however, the bands split or the weight even appears incoherent. This reflects the additional

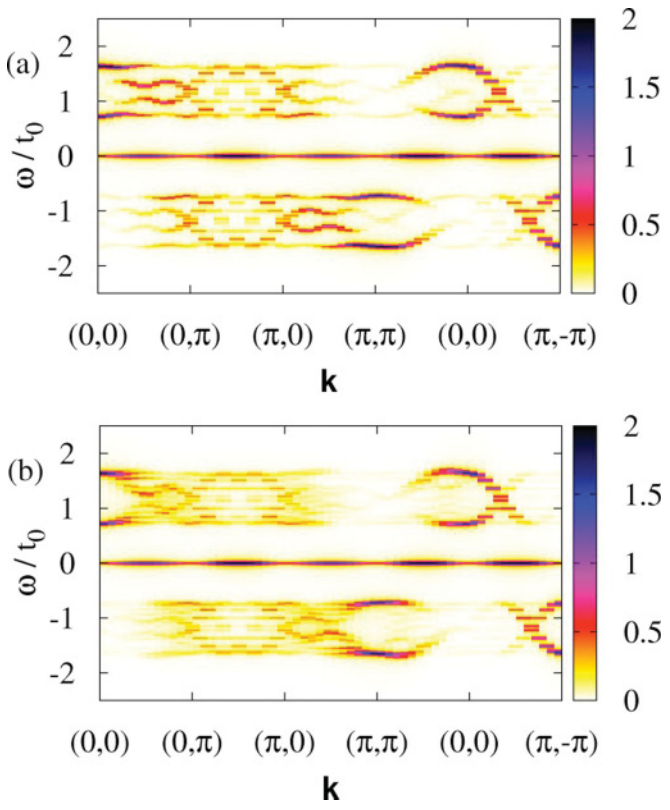

FIG. 8. (Color online) Spectral density $A(\mathbf{k},\omega)$ for two patterns of the $SOS_{1/3}$ phase at $\lambda = 0$. The $L_x \times L_y = 24 \times 24$ lattice is used, and the E-AF domains run in the (1,1) direction, from (0,0) to (24,24). Periodic boundary conditions are employed, and peaks were broadened with a Lorentzian with a width $\delta = 0.02t_0$.

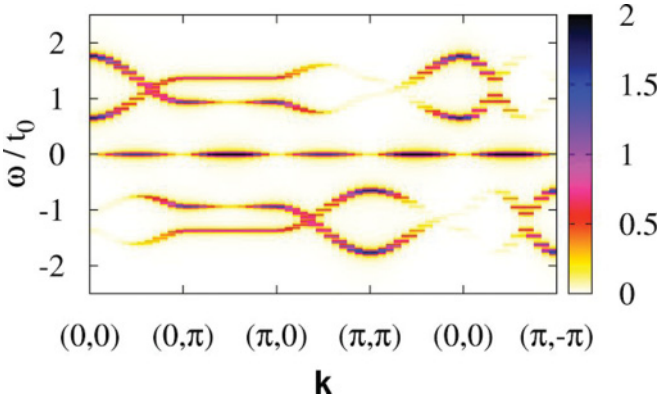

FIG. 9. (Color online) Spectral density $A(\mathbf{k},\omega)$ for an artificial reference model where all hoppings are replaced by their absolute values; this phase has the same energy as the $SOS_{1/3}$ phase. Parameters are as in Fig. 8.

modulation of the hoppings by the complex Berry phase, which can lead to superstructures and to effective disorder. As one can infer from the density of states, see Fig. 7, spectral weight is not only shifted to different momenta in different $SOS_{1/3}$ configurations, but also transferred between different energies.

The dimensional reduction unveiled here appears linked to the dispersionless edge states of the E-AF phase,[6,39] which are unoccupied in the $SOS_{1/n}$ phases [see the delta peak in the density of states, Fig. 7, and the dispersionless states in $A(\mathbf{k},\omega)$ in Fig. 8]. While the one-particle energies of the occupied bands change, the dispersionless states are unaffected by flipping a stripe. The "$SOS_{1/2}$" phase,[12] and the modified phase of Fig. 4(c) do not have such dispersionless states and do also not have degenerate states, and we will thus analyze the dispersionless states and their impact on the $SOS_{1/3}$ phase.

In finite E-AF clusters, the dispersionless states are $z^2 - x^2$ and $y^2 - z^2$ orbitals localized on sites along the edge. These $z^2 - x^2$ ($y^2 - z^2$) orbitals are localized because their orbital symmetry only permits them to hop to a single site, their neighbor in the x-(y-)direction, but this bond is AF, and hopping is thus suppressed by the magnetic order. In the bulk, the bond in the opposite direction would be FM, and the orbital can thus delocalize, but this bond is missing at the cluster edge. If one considers a single stripe of the $SOS_{1/3}$ phase as an isolated E-AF domain, then the electrons can only delocalize within (i) both orbitals of the central site and (ii) the directional orbitals pointing toward it on the two wings [these orbitals are shown in Fig. 6]. The orthogonal (planar) orbitals on the wings do not hybridize with any other orbital of the stripe and are the localized edge states, which are empty at $x = 1/3$.

As discussed above in Sec. IV B, however, hopping *between* the stripes is not suppressed and the arrows on adjacent stripes are thus coupled. As illustrated in Fig. 10, electrons in the planar orbitals can hop to the directional orbital on the wing site of an adjacent stripe. This leads to the subsystem consisting of the six orbitals drawn with black lines in Fig. 10. After taking into account reflection symmetry with respect to the central

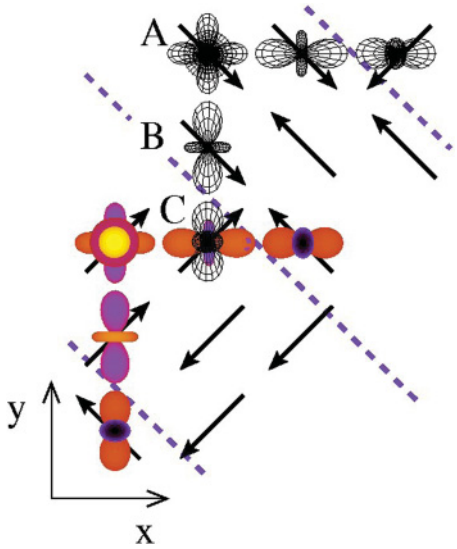

FIG. 10. (Color online) Two orbital building blocks of the $SOS_{1/3}$ phase. Black arrows give the $SOS_{1/3}$ spin pattern and dashed lines indicate the stripes. Orbitals shown with shading/lines illustrate the unit cells corresponding to two arrows in adjacent stripes. Site A is a "center" site with occupancy in both the $x^2 - y^2$ and the $3z^2 - r^2$ orbitals, site B is a "wing" site, only the more highly occupied $3y^2 - r^2$ orbital is shown. Site C is also a "wing" site, but here both orbitals are shown, the planar $y^2 - z^2$ orbital is drawn with lines and the directional $3x^2 - r^2$ with shading. An electron in the planar $y^2 - z^2$ orbital can *only* hop along $+y$ to site B of the adjacent stripe: It cannot hop along the x-direction due to its orbital symmetry (Ref. 1), and it cannot hop along the $-y$ bond due to the AF spins.

site, the even and odd subspace each yields a 3×3 matrix

$$H_{e/o} = \begin{pmatrix} 0 & -t_{e/o} & 0 \\ -t_{e/o} & 0 & -\frac{\sqrt{3}t_0}{2\sqrt{2}}e^{i\phi} \\ 0 & -\frac{\sqrt{3}t_0}{2\sqrt{2}}e^{-i\phi} & 0 \end{pmatrix}, \qquad (6)$$

where subscripts e/o denote the even and odd subspace, $t_{e,o}$ is given by $\frac{t_0}{2}$ for the even case and $\frac{t_0\sqrt{3}}{2}$ for the odd case, and ϕ denotes the complex Berry phase. It can be easily seen that such a matrix always has one eigenvalue $\epsilon = 0$ and that the corresponding eigenvector only lives on the first and third sites. Here, this implies that the directional orbital on the wing sites has no overlap with dispersionless states. The only process connecting the building blocks described by Eq. (6) is the hopping $-\frac{t_0}{2\sqrt{2}}e^{-i\phi}$ between two directional orbitals sitting on wing sites belonging to adjacent stripes, e.g., between the $3y^2 - r^2$ orbital on site B and the $3x^2 - r^2$ orbital on site C in Fig. 10. Since it only acts on the directional orbitals, which are not involved in the $\epsilon = 0$ states, the latter are not affected and remain dispersionless in the $SOS_{1/3}$ phase. In the "$SOS_{1/2}$" phase,[12] the E-phase domains are too narrow to support dispersionless states and in the modified phase of Fig. 4(c), where the "arrows" of the E phase point in opposite directions in adjacent domains, the different orbital pattern shown in Fig. 6 also prevents similar dispersionless states.

Such a protection of a large ground-state degeneracy by dispersionless states is reminiscent of spin ice, where flat bands enforce the ice rules.[40] The notion that the protection of a degeneracy is caused by the dispersionless states at $\omega = 0$ can be motivated by observing that the lack of dispersion implies that the states are completely localized and do not communicate with other, dispersive, states. The energy of the occupied subband centered around $\omega = -\epsilon \approx -1.2t_0$ can then only be affected by processes involving the symmetric unoccupied states at $\omega = +\epsilon$. Treating the hybridization between these two subbands in perturbation theory, valid for large energy differences $2\epsilon > \frac{t_0}{2\sqrt{2}}$, the second-order contribution can be shown to be independent of the hopping's complex phase and the third-order contribution drops out entirely. If hybridization sensitive to the Berry phase then occurs almost exclusively within the occupied subband, the individual one-particle energies seen in the density of states can be changed, but the total energy cannot, because all energy gained by one state is lost by another.

V. DISCUSSION AND CONCLUSIONS

The E-AF phase, which provides the stripe building blocks, displays FE polarization due to exchange striction.[41,42] Additionally, the many bonds with noncollinear spins lead to a sizable Dzyaloshinskii-Moriya interaction. We found that the FE polarization caused by the latter is larger in some configurations and smaller in others. This causes an additional energy difference, but as long as it is small compared to the energy separating the $SOS_{1/3}$ ground-state manifold from excited states, this should not qualitatively alter the physical behavior that we described here. On the other hand, the different FE properties might provide a handle to manipulate the stripes. It should finally be noted that the multiferroic properties of a large collection of nearly degenerate states differing by the FE polarization has not been investigated thus far and may be highly nontrivial due to potential interference effects.

To conclude, we have studied a model Hamiltonian appropriate for narrow-band manganites at small Jahn-Teller coupling using unbiased numerical techniques. We found that the spins of the 2D system spontaneously undergo dimensional reduction into 1D stripes for dopings $1/3$, $1/4$, . . . Adjacent stripes always have spins at a 90° angle, but the spins of stripes at larger distances are not correlated. The electronic kinetic energy, on the other hand, remains fully 2D. This indicates that the manganite results described here induce the spins to behave in a way analogous to the (orbital pseudo-) spins in the so-called compass model, which is also used to describe protected qbits. However, in contrast to the compass model, our model Hamiltonian does not commute with the corresponding symmetry operators, and the effect is thus an *emergent* property of the ground-state manifold.

ACKNOWLEDGMENTS

S.L., C.Ş., and E.D. were supported by the US Department of Energy, Office of Basic Energy Sciences, Materials Sciences and Engineering Division. S.D. was supported by the 973 Projects of China (Grant No. 2011CB922101) and the NSFC (Grant No. 11004027). M.D. acknowledges support by the Deutsche Forschungsgemeinschaft under the Emmy-Noether program and helpful discussions with Z. Nussinov.

*m.daghofer@ifw-dresden.de

[1] E. Dagotto, T. Hotta, and A. Moreo, Phys. Rep. **344**, 1 (2001).
[2] S.-W. Cheong and M. Mostovoy, Nat. Mater. **6**, 13 (2007).
[3] D. Khomskii, Physics **2**, 20 (2009).
[4] K. F. Wang, J.-M. Liu, and Z. F. Ren, Adv. Phys. **58**, 321 (2009).
[5] T. Hotta, A. Feiguin, and E. Dagotto, Phys. Rev. Lett. **86**, 4922 (2001).
[6] T. Hotta, M. Moraghebi, A. Feiguin, A. Moreo, S. Yunoki, and E. Dagotto, Phys. Rev. Lett. **90**, 247203 (2003).
[7] R. Kajimoto, H. Yoshizawa, H. Kawano, H. Kuwahara, Y. Tokura, K. Ohoyama, and M. Ohashi, Phys. Rev. B **60**, 9506 (1999).
[8] T. Kimura, K. Hatsuda, Y. Ueno, R. Kajimoto, H. Mochizuki, H. Yoshizawa, T. Nagai, Y. Matsui, A. Yamazaki, and Y. Tokura, Phys. Rev. B **65**, 020407 (2001).
[9] C. D. Ling, J. E. Millburn, J. F. Mitchell, D. N. Argyriou, J. Linton, and H. N. Bordallo, Phys. Rev. B **62**, 15096 (2000).
[10] J. van den Brink and D. Khomskii, Phys. Rev. Lett. **82**, 1016 (1999).
[11] S. Dong, R. Yu, J.-M. Liu, and E. Dagotto, Phys. Rev. Lett. **103**, 107204 (2009).
[12] G. Giovannetti, S. Kumar, J. van den Brink, and S. Picozzi, Phys. Rev. Lett. **103**, 037601 (2009).
[13] S. E. Sebastian, N. Harrison, C. D. Batista, L. Balicas, M. Jaime, P. A. Sharma, N. Kawashima, and I. R. Fisher, Nature **441**, 617 (2006).
[14] S. T. Bramwell and M. J. P. Gingras, Science **294**, 1495 (2001).
[15] Y. Tabata, H. Kadowaki, K. Matsuhira, Z. Hiroi, N. Aso, E. Ressouche, and B. Fåk, Phys. Rev. Lett. **97**, 257205 (2006).
[16] R. Moessner and S. L. Sondhi, Phys. Rev. B **68**, 064411 (2003).
[17] K. I. Kugel and D. I. Khomskiĭ, Soviet Physics Uspekhi **25**, 231 (1982).
[18] A. Mishra, M. Ma, F.-C. Zhang, S. Guertler, L.-H. Tang, and S. Wan, Phys. Rev. Lett. **93**, 207201 (2004).
[19] Z. Nussinov and E. Fradkin, Phys. Rev. B **71**, 195120 (2005).
[20] Z. Nussinov and G. Ortiz, Proc. Natl. Acad. Sci. USA **106**, 16944 (2009).
[21] L. Cincio, J. Dziarmaga, and A. M. Oleś, Phys. Rev. B **82**, 104416 (2010).
[22] J. van den Brink, P. Horsch, F. Mack, and A. M. Oleś, Phys. Rev. B **59**, 6795 (1999).
[23] Z. Nussinov, M. Biskup, L. Chayes, and J. van den Brink, Europhys. Lett. **67**, 990 (2004).
[24] A. van Rynbach, S. Todo, and S. Trebst, Phys. Rev. Lett. **105**, 146402 (2010).
[25] G. Jackeli and G. Khaliullin, Phys. Rev. Lett. **102**, 017205 (2009).
[26] J. Chaloupka, G. Jackeli, and G. Khaliullin, Phys. Rev. Lett. **105**, 027204 (2010).
[27] F. Trousselet, A. Oleś, and P. Horsch, Europhys. Lett. **91**, 40005 (2010).
[28] B. Douçot, M. V. Feigel'man, L. B. Ioffe, and A. S. Ioselevich, Phys. Rev. B **71**, 024505 (2005).
[29] S. Gladchenko, D. Olaya, E. Dupont-Ferrier, B. Douçot, L. B. Ioffe, and M. E. Gershenson, Nat. Phys. **5**, 48 (2008).
[30] Z. Nussinov, C. D. Batista, and E. Fradkin, Int. J. Mod. Phys. **20**, 5239 (2006).
[31] Z. Nussinov and G. Ortiz, Ann. Phys. **324**, 977 (2009).
[32] E. Müller-Hartmann and E. Dagotto, Phys. Rev. B **54**, R6819 (1996).
[33] R. Yu, S. Yunoki, S. Dong, and E. Dagotto, Phys. Rev. B **80**, 125115 (2009).
[34] J. Salafranca, G. Alvarez, and E. Dagotto, Phys. Rev. B **80**, 155133 (2009).
[35] S. Dong, R. Yu, S. Yunoki, J.-M. Liu, and E. Dagotto, Phys. Rev. B **78**, 155121 (2008).
[36] J. Riera, K. Hallberg, and E. Dagotto, Phys. Rev. Lett. **79**, 713 (1997).
[37] M. Yamanaka, W. Koshibae, and S. Maekawa, Phys. Rev. Lett. **81**, 5604 (1998).
[38] J. van den Brink, G. Khaliullin, and D. I. Khomskii, Phys. Rev. Lett. **83**, 5118 (1999).
[39] T. Hotta, Rep. Prog. Phys. **69**, 2061 (2006).
[40] S. V. Isakov, R. Moessner, and S. L. Sondhi, Phys. Rev. Lett. **95**, 217201 (2005).
[41] I. A. Sergienko, C. Şen, and E. Dagotto, Phys. Rev. Lett. **97**, 227204 (2006).
[42] S. Picozzi, K. Yamauchi, B. Sanyal, I. A. Sergienko, and E. Dagotto, Phys. Rev. Lett. **99**, 227201 (2007).